JOURNAL OF SOLID STATE CHEMISTRY **132,** 182–187 (1997)
ARTICLE NO. SC 977441

Crystal Structure and Magnetic Properties of $Bi_{0.267}Pr_{0.733}SrO_{3-\delta}$ via Neutron Diffraction

M. Wołcyrz[1] and R. Horyń

Institute of Low Temperature and Structure Research, Polish Academy of Sciences, ul. Okólna 2, 50-950 Wrocław 2, Poland

and

G. André and F. Bourée

Laboratoire Léon Brillouin (CEA-CNRS), CEA-Saclay, 91191 Gif-sur-Yvette Cedex, France

Received August 19, 1996; in revised form April 21, 1997; accepted April 22, 1997

The crystal structure of $Bi_{0.267}Pr_{0.733}SrO_{2.963}$ has been refined based on neutron powder diffraction data (monoclinic system, $P12_1/n1$ space group, $a=5.9728(2)$ Å, $b=6.1143(2)$ Å, $c=8.5308(3)$ Å, $\beta=89.92(1)^\circ$ at $T=300$ K). A nonhomogeneous occupation of atomic positions has been obtained. Down to $T=1.4$ K, no magnetic ordering has been observed on $Bi_{0.267}Pr_{0.733}SrO_{2.963}$ neutron powder diffraction diagrams. This result is consistent with the AC-susceptibility vs T curve, which shows paramagnetic behavior down to 4.2 K. © 1997 Academic Press

INTRODUCTION

There is relatively much data in the literature concerning $PrBaO_3$, whereas $PrSrO_3$ seems to be almost completely omitted. The main reason is probably the multiphase nature of $PrSrO_3$ samples. The crystal structure and magnetic properties of $PrBaO_3$ were characterized by Jacobson *et al.* (1), Cao *et al.* (2), Rosov *et al.* (3), Felner *et al.* (4), and Hinatsu (5). At present it seems to be well established that $PrBaO_3$ crystallizes in orthorhombic *Pbnm* space group with $a \approx b \approx \sqrt{2}a_p$, $c \approx 2a_p$, where $a_p \approx 4$ Å denotes perovskite unit cell parameter. According to Felner *et al.* (4) $PrBaO_3$ orders antiferromagnetically at 11.7 K with a slight ferromagnetic component due to a canting of Pr moments.

In our previous paper (6) we reported on the synthesis and crystallochemical characterization of the binary $PrSrO_3$-type phase as well as on its Bi/Pr-substituted solid solution $Pr_{1.1(1-x)}Bi_{0.8x}Sr_{0.9+0.3x}O_{2.932+0.094x}$ $(0 \le x \le 0.5)$. We have shown that unlike $PrBaO_3$, the Sr-compound appears to be off-stoichiometric and should be described as $Pr(Sr_{0.9}Pr_{0.1})O_{3-\delta}$. The crystal structure is a monoclinically distorted perovskite-type atomic arrangement identical to that occurring in a large group of $REBiSr_2O_6$-type ternaries (7, 8). The same is true for the solid solution mentioned above. We have also found, that contrary to our expectations, this solid solution extends within the ternary oxide system Bi–Pr–Sr–O toward the binary compound $Bi_2Sr_3O_6$ instead of to its second natural terminus $BiPrSr_2O_6$, which does not exist. Characteristic features of this solid solution are the following: (i) the effective valency (V_{eff}) of the average Bi/Pr ion increases vs bismuth contribution instead of remaining constant (+4) as in the Bi/Tb-substituted solid solution based on a $TbSrO_3$ matrix (9); (ii) the structure deficiency increases vs x and results in vacancies formed in both the oxygen (~2%) and praseodymium (~1.5%) sublattices. Based on the precise density and valency measurements, the most probable distribution of the structure components and the vacancies in the crystal structure of this solid solution were postulated (6).

The aim of the present work was to refine the crystal structure of the solid solution under consideration. This was of interest because the postulated structural model appeared to be different from that characteristic of the vacancy-free homologous solid solution of $Tb_{1-x}Bi_xSrO_3$-type (9), recently determined with neutrons on an $x = 0.2$ sample (10). Moreover, the use of neutron radiation, which distinctly differentiates Bi and Pr scattering amplitudes, makes possible the precise determination of occupation numbers for the Bi/Pr and Sr/Pr atomic positions.

SAMPLE CHARACTERIZATION

From the entire domain of homogeneity reflected by the formula $Pr_{1.1(1-x)}Bi_{0.8x}Sr_{0.9+0.3x}O_{2.932+0.094x}$ $(0 \le x \le 0.5)$, one composition (namely $Pr_{0.733}Bi_{0.267}SrO_{2.963}$) was chosen for crystal structure analysis. The reason for this

[1]To whom correspondence should be addressed.

0022-4596/97 $25.00

choice is that the stoichiometry of the sample matches exactly the crossing of the Pr and Tb solid solutions (6, 9).

Samples were prepared using Johnson–Mathey 3 N purity Bi_2O_3, Pr_6O_{11}, and $SrCO_3$. Appropriate mixtures of these reagents were calcinated in air at 800°C for 24 h, reground, pelletized and sintered in air at 900°C for 48 h and calcinated in air once again at 900°C for 72 h. In all these operations, alumina boats were used as sample holders.

The basic crystallographic parameters of the $Pr_{0.733}Bi_{0.267}SrO_{2.963}$ sample determined in (6) are

$$a = 5.971(6)\ \text{Å},\ b = 6.118(6)\ \text{Å},\ c = 8.542(8)\ \text{Å},\ \beta = 90.10(9)^\circ,$$

$$d_m = 6.21(6)\ \text{g/cm}^3,\ V_{\text{eff}} = 3.92,\ Z_{\text{eff}} = 3.967,$$

whereas the most probable distribution of the elements and vacancies through all 24 atomic positions available in the unit cell can be described as

$$[Pr_{2.875}Bi_{1.057}\square_{0.066}]\ [Sr_{3.966}Pr_{0.033}]\ [O_{11.754}\square_{0.245}], \quad [1]$$

where three expressions in brackets refer to three different occupied crystallographic sites and □-sign denotes lattice vacancies. The formula [1] has been a subject of verification with the neutron data.

EXPERIMENTAL

Neutron powder diffraction diagrams have been measured on the 3T2 and G4.1 2-axis spectrometers of the LLB, Saclay (ORPHEE Reactor). The 3T2 is a high resolution powder diffractometer, with a Ge (335) monochromator ($\lambda = 1.2272$ Å) and 20 ^{3}He detectors. The G4.1 is equipped with a vertical, focusing graphite (002) monochromator ($\lambda = 2.4249$ Å) and a linear position sensitive BF_3 detector resolved to 800 cells. The neutron diffraction diagrams were obtained at $T = 300$ K in the 13–120° 2θ-range on 3T2 and at $T = 1.4$ K and $T = 39$ K on G4.1 (13–93° 2θ-range). The crystal structure was refined by the Rietveld technique using the FULLPROF program (11).

AC-magnetic susceptibility curves of $Bi_{0.267}Pr_{0.733}SrO_{2.963}$ and $Pr_{0.55}Sr_{0.45}O_3$ samples (to compare with bismuth-free terminus) were collected with a Lake Shore AC-Susceptometer 7000. The data were taken for amplitudes of the AC-field equal to 10 Gs at a frequency of 111.1 Hz on heating of the samples after having cooled them under zero field.

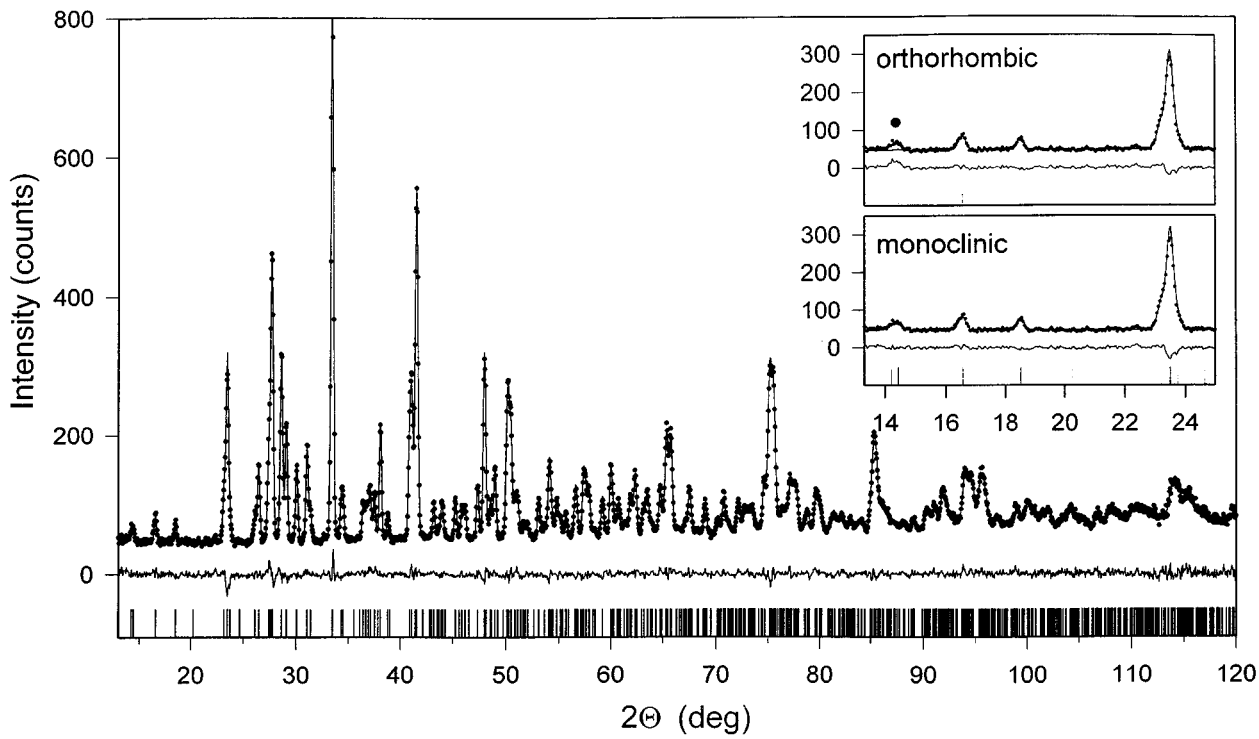

FIG. 1. High-resolution powder diffraction diagram (circles) and Rietveld refinement fit (solid line) of $Bi_{0.267}Pr_{0.733}SrO_{2.963}$ for $\lambda = 1.2272$ Å neutrons at $T = 300$ K (3T2 diffractometer) (top), differential diagram (middle), and theoretical peak positions (bottom). Insets show the magnified low-angle region obtained in the course of the structure refinement in orthorhombic (*Pbnm*) and monoclinic ($P12_1/n1$) space groups. A crucial group of peaks influencing the choice of symmetry is marked by a circle.

TABLE 1

Lattice Parameters (a, b, c, β), Calculated and Measured Sample Densities (d_x, d_m), Wyckof Positions, Atomic Positional Parameters (x, y, z), Isotropic Temperature Factors (B), Occupancies (n), and Agreement Factors (R_p, R_{wp}, R_B, χ^2) for $Bi_{0.267}Pr_{0.733}SrO_{2.963}$ at 300 K

Atom	Pos.	x	y	z	B	n
Sr(1)	4(*e*)	0.9898(4)	0.4548(2)	0.7498(7)	0.82(3)	1
Pr(1)	2(*a*)	0	0	0	0.35(3)	0.974(20)
Bi(1)	2(*a*)	0	0	0	0.35(3)	0.026(20)
Pr(2)	2(*b*)	0	0	0.5	0.35(3)	0.492(20)
Bi(2)	2(*b*)	0	0	0.5	0.35(3)	0.508(20)
O(1)	4(*e*)	0.3985(4)	0.5404(4)	0.7549(9)	0.94(4)	0.988
O(2)	4(*e*)	0.2925(9)	0.8039(10)	0.4484(8)	1.56(12)	0.988
O(3)	4(*e*)	0.1946(8)	0.2935(9)	0.4452(7)	0.79(4)	0.988

$R_p = 3.58\%$; $R_{wp} = 4.13\%$; $R_B = 3.51\%$; $\chi^{22} = 1.94$

Note. Space group: $P12_1/n1$; $a = 5.9728(2)$ Å, $b = 6.1143(2)$ Å, $c = 8.5308(3)$ Å, $\beta = 89.92(1)^\circ$. $d_x = 6.27$ g/cm^3; $d_m = 6.21$ g/cm^3.

TABLE 2

Interatomic Distances (Å) in $Bi_{0.267}Pr_{0.733}SrO_{2.963}$

Pr(1)/Bi(1)–O(1)	2.27	×2
Pr(1)/Bi(1)–O(2)	2.28	×2
Pr(1)/Bi(1)–O(3)	2.27	×2
Pr(2)/Bi(2)–O(1)	2.19	×2
Pr(2)/Bi(2)–O(2)	2.16	×2
Pr(2)/Bi(2)–O(3)	2.19	×2
Sr–O(1)	2.50	
	2.62	
	3.57	
	3.64	
Sr–O(2)	2.54	
	2.87	
	3.03	
	3.80	
Sr–O(3)	2.52	
	2.86	
	3.04	
	3.82	

CRYSTAL STRUCTURE AT ROOM TEMPERATURE

The crystal structure of $Bi_{0.267}Pr_{0.733}SrO_{2.963}$ was refined from neutron powder diffraction data taken at $T =$ 300 K (3T2 diffractometer) and at $T = 39$ K (G4.1 diffractometer). In order to simplify the refinement process, a vacancy-free structure model was applied. Therefore, the main problem to solve was the choice of proper symmetry (orthorhombic or monoclinic). By analogy to $BaPrO_3$, $Bi_{0.267}Pr_{0.733}SrO_{2.963}$ seems to be described by space group *Pbnm*, but our previous X-ray powder diffraction studies (6) indicated a monoclinic distortion and the most probable structure model found earlier for $BiNdSr_2O_6$ ($P12_1/n1$ space group) (7). Therefore, we decided to refine the structure in both groups. The differences in the reliability factors in both cases were very small, with a slight advantage for the monoclinic model. We obtained the most convincing argument from a comparison of the low-angle range of the diffraction diagrams calculated during Rietveld refinement in orthorhombic and monoclinic symmetries. The measured diagram contained some reflections which are absent in the orthorhombic symmetry, but which could be successfully generated in the monoclinic one (cf. insets in Fig. 1). Therefore our choice was $P12_1/n1$. The results of the refinement are presented in Table 1.

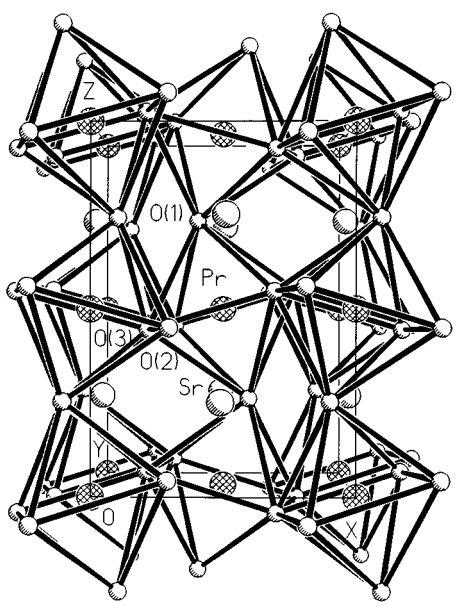

FIG. 2. Perspective view of the $Bi_{0.267}Pr_{0.733}SrO_{2.963}$ unit cell. Note that in the real structure, mixed occupations of all Pr and Bi positions are observed.

The structure of $Bi_{0.267}Pr_{0.733}SrO_{2.963}$ (Fig. 2) is in agreement with those obtained for other orthorhombic perovskites. Nonhomogeneous occupations have been obtained for Bi and Pr atoms in 2(*a*) (0, 0, 0) and 2(*b*) (0, 0, 1/2) Wyckoff positions, with the 2(*a*) site almost fully occupied by Pr. As in $BaPrO_3$ (1), the oxygen environment of Sr is considerably distorted, but the $(Pr/Bi)O_6$ octahedra remain almost regular (cf. Table 2). In comparison with the prototype $BiNdSr_2O_6$ structure (7) in which Nd–O and Bi–O distances of the MO_6 octahedra are equal to 2.32–2.35 and 2.09–2.12 Å, respectively, the Pr(1)/Bi(1)–O distances (2.27–2.28 Å) are shorter, whereas the Pr(2)/Bi(2)–O ones (2.16–2.19 Å) are slightly longer. This is in agreement with occupancies found for appropriate mixed atomic positions: the Bi contribution to the Pr(1) position decreases Pr–O bond lengths, whereas the Pr contribution to the Bi(2) increases Bi–O bond lengths.

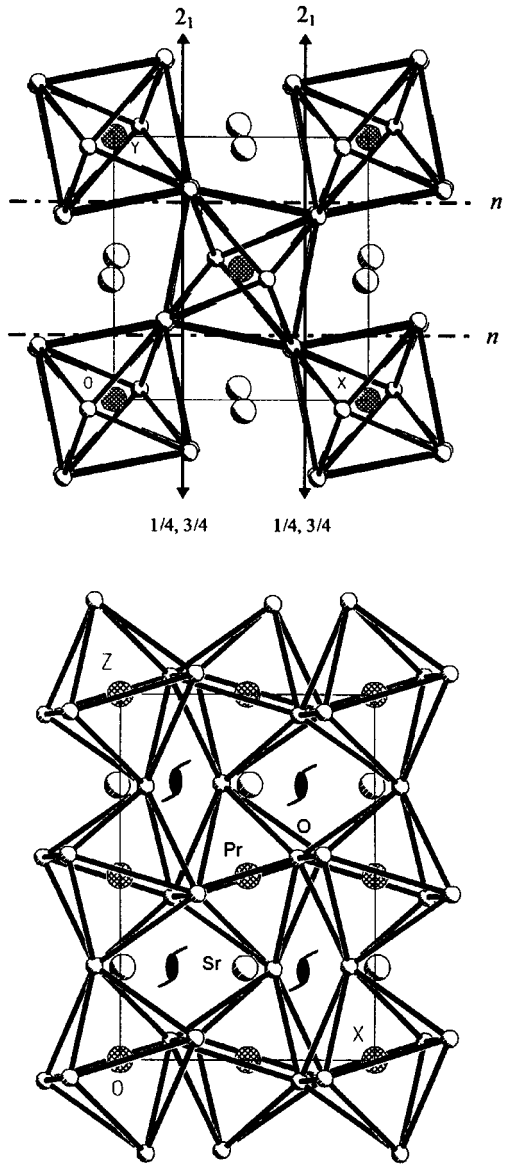

FIG. 3. Projection of the $Bi_{0.267}Pr_{0.733}SrO_{2.963}$ structure on ***ab*** (top) and ***ac*** (bottom) unit cell planes. The figure shows the symmetry elements of the $P12_1/n1$ space group. Note that in the top drawing, MO_6 octahedra are rotated by a very small angle around the *z*-axis.

Figure 3 illustrates the difference between $Bi_{0.267}Pr_{0.733}SrO_{2.963}$ and $BaPrO_3$ described in $P12_1/n1$ and *Pbnm* symmetries, respectively. The monoclinic symmetry allows two types of PrO_6 octahedra (forming an array running along the *z*-axis) to rotate around *z* independently. This results in a very slight smearing of the octahedra visible in the top drawing of Fig. 3. In the *Pbnm* space group, mirror planes perpendicular to *z* exist instead of 2_1-axes at $z = 1/4$ and 3/4, as shown in bottom drawing of Fig. 3. Having less freedom, the octahedra mutually overlap on the ***ab*** projection.

Considering the vacancy-containing structure model proposed in (6) (cf. formula [1]), a comparative refinement was also undertaken. Prior to the refinement, the formula had been modified in order to take into account the final results obtained for the vacancy-free model. The modification consisted of splitting the $[Pr_{2.875}Bi_{1.057}\square_{0.066}]$ assemblage into the two atomic sites found (2(*a*) and 2(*b*)) with the M-type vacancies ($\square_{0.066}$) located in the 2(*a*) position occupied by Pr atoms, namely,

$$[Pr_{1.933}\square_{0.066}][Bi_{1.057}Pr_{0.943}]\,[Sr_{3.966}Pr_{0.033}]\,[O_{11.754}\square_{0.245}]. \quad [2]$$

Note that the formula [2] reflects an atomic distribution which is almost identical to the basic result obtained directly from neutron Rietveld refinement, namely,

$$[Pr_{1.948}Bi_{0.052}][Bi_{1.016}Pr_{0.984}]\,[Sr_4][O_{11.856}\square_{0.144}]. \quad [3]$$

As a consequence, the Rietveld refinement performed for the structure model [2] has given a fit of comparable quality to that of the vacancy-free one ($R_p = 3.62\%$; $R_{wp} = 4.16\%$; $R_B = 3.57\%$; $\chi^2 = 1.97$). Taking into account the experimental and calculated densities ($d_m = 6.21$ g/cm^3; $d_x = 6.22$ and 6.27 g/cm^3 for the vacancy-containing and vacancy-free models, respectively), the vacancy-containing model must, in principle, be treated as the more appropriate one.

SEARCH FOR MAGNETIC ORDERING AT LOW TEMPERATURES

In order to determine if any magnetic ordering similar to that found in $PrBaO_3$ (4) takes place at low temperature in $Bi_{0.267}Pr_{0.733}SrO_{2.963}$, AC-magnetic susceptibility down to 4.2 K and neutron powder diffraction at 1.4 K (G4.1 diffractometer) were measured.

The AC–magnetic susceptibility curves of $Bi_{0.267}Pr_{0.733}SrO_{2.963}$ and of the terminal $Pr_{0.55}Sr_{0.45}O_3$ sample are shown in Fig. 4. Both samples exhibit paramagnetic behavior over the entire range of the temperature measured (4.2–300 K) which can be described by the modified Curie–Weiss law: $\chi = \chi_0 + (C/(T - \Theta))$. The susceptibility curve of the $Pr_{0.55}Sr_{0.45}O_3$ terminal sample bears an evident sign of a magnetic anomaly taking place at about 8 K. It seems to possess a similar kind of ordering to $PrBaO_3$ which orders antiferromagnetically at about 12 K (4). However, presence of diamagnetic bismuth weakens the effect and the ordering becomes undetectable in the susceptibility curve of the $Bi_{0.267}Pr_{0.733}SrO_{2.963}$ sample.

A least square fit of the AC-susceptibility curves to the modified Curie–Weiss law has enabled us to evaluate following basic parameters for these two compositions, namely, $Pr_{0.55}Sr_{0.45}O_3$: $\chi_0 = 1.2 \times 10^{-3}$ emu/at. Pr, $\Theta = 6.7$ K, $C = 0.186$ emu · K/at. Pr, $\mu_{eff} = 1.22\ \mu_B$, $Pr_{0.267}Sr_{0.733}O_{2.963}$: $\chi_0 = 1.642 \times 10^{-3}$ emu/at. Pr, $\Theta = -15.0$ K, $C = 0.151$ emu · K/at. Pr, $\mu_{eff} = 1.10\ \mu_B$.

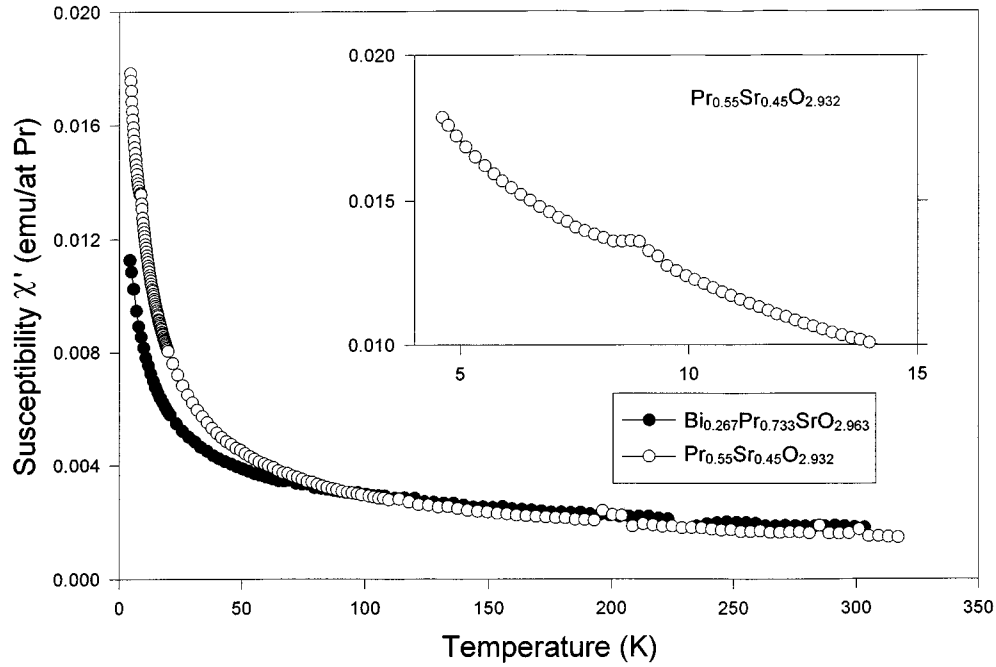

FIG. 4. AC–magnetic susceptibility curves for $Pr_{0.55}Sr_{0.45}O_3$ (open circles) and $Bi_{0.267}Pr_{0.733}SrO_{2.963}$ (filled circles).

As seen, the effective magnetic moments are in an evident contradiction to those resulting from the Hund's rule for Pr^{+3} (3.58 μ_B) and Pr^{+4} (2.54 μ_B). Considering the results of iodometric titration performed in (6) for several compositions of the solid solution studied (including $Bi_{0.267}Pr_{0.733}SrO_{2.963}$), a strong crystal field effect should be taken into account to explain the origin of such a strong reduction of the μ_{eff}.

An additional check for magnetic ordering at low temperatures was made by comparing the G4.1 neutron powder diffraction diagrams taken at $T = 1.4$ K and T = 39 K. Within experimental errors, the refined parameters obtained are identical at both temperatures. Figure 5 shows the results of the Rietveld refinement at $T = 1.4$ K, together with the difference between the $T = 1.4$ K and $T = 39$ K diagrams. As can be seen, the differences in the $y_{obs}(1.4\text{ K})$–$y_{obs}(39\text{ K})$ curve are much smaller than those given by the $y_{obs}-y_{calc}$ diagram. In fact, any attempt to introduce a magnetic ordering did not improve the quality of the fit. This means that the maximum value of a magnetic moment exhibited below 39 K, cannot exceed 0.15 μ_B/Pr.

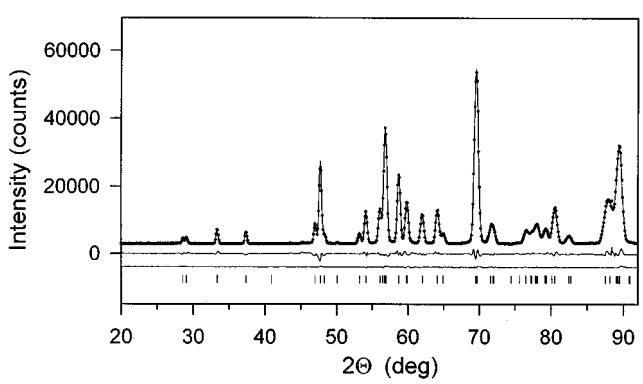

FIG. 5. Rietveld refinement plot for $Bi_{0.267}Pr_{0.733}SrO_{2.963}$ at 1.4 K (G4.1 diffractometer): circles, experimental data (y_{obs}); solid line, calculated diagram (y_{calc}); sticks, peak positions. Two differential diagrams are shown: $y_{obs} - y_{calc}$ (above) and $y_{obs}(T = 1.4\text{ K}) - y_{obs}(T = 39\text{ K})$ (below).

ACKNOWLEDGMENTS

This work was supported by State Committee for Scientific Research (Grant 3 T09A 122 08) and Human Capital and Mobility—Access to Large Scale Facilities PECO Extension Program (Contract ERB CIPD CT 940080).

REFERENCES

1. A. J. Jacobson, B. C. Tofield, and B. E. F. Fender, *Acta Crystallogr. B* **28,** 956 (1972).
2. G. Cao, Tan Yuen, P. Pernambuco-Wise, J. E. Crow, J. W. O'Reilly, M. V. Kuric, R. P. Guertin, N. Rosov, and J. W. Lynn, *J. Appl. Phys.* **70,** 6332 (1991).
3. N. Rosov, J. W. Lynn, Q. Lin, G. Cao, J. W. O'Reilly, P. Pernambuco-Wise, and J. W. Crow, *Phys. Rev. B* **45,** 982 (1992).
4. I. Felner, Y. Yeshurun, G. Hilscher, T. Holubar, G. Schaudy, U. Yaron, O. Cohen, Y. Wolfus, E. R. Yacoby, L. Klein, F. H. Potter, C. S. Rastomjee, and R. G. Egdell, *Phys. Rev. B* **46,** 9132 (1992).
5. Y. Hinatsu, *J. Solid. State Chem.* **102,** 362 (1993).

6. R. Horyń, M. Wołcyrz, and Z. Bukowski, *J. Solid State Chem.* **124,** 176 (1996).
7. A. Lenz and Hk. Müller-Buschbaum, *J. Less-Common Met.* **161,** 141 (1990).
8. R. Horyń, M. Wołcyrz, A. Wojakowski, and A. J. Zaleski, *J. Alloys Comp.* **242,** 35 (1996).
9. R. Horyń, Z. Bukowski, and M. Wołcyrz, *J. Solid State Chem.* **122,** 321 (1996).
10. M. Wołcyrz, R. Horyń, G. André, and F. Bourée, *Phys. Rev. B* **55,** 14335 (1997).
11. J. Rodriguez-Carvajal, *Physica B* **192,** 55 (1993).